The Journal of Experimental Biology **198**, 585–602 (1995)
Printed in Great Britain © The Company of Biologists Limited 1995

SPEED EFFECTS ON MIDLINE KINEMATICS DURING STEADY UNDULATORY SWIMMING OF LARGEMOUTH BASS, *MICROPTERUS SALMOIDES*

BRUCE C. JAYNE[1] AND GEORGE V. LAUDER[2]

[1]*Department of Biological Sciences, University of Cincinnati, Cincinnati, OH 45221-0006, USA* and
[2]*Department of Ecology and Evolutionary Biology, University of California, Irvine, CA 92717, USA*

Accepted 3 October 1994

Summary

We used frame-by-frame analysis of high-speed videotapes to quantify midline kinematics during steady swimming in largemouth bass at five standardized speeds (0.7, 1.2, 1.6, 2.0 and 2.4 $L\,s^{-1}$, where L is total length). By combining morphological data from X-ray photographs with mathematical reconstructions of the midline of each fish, we determined the amplitude and timing of lateral displacement (z_{max}), lateral flexion (β_{max}) and the angle between the midline and the axis of forward travel (θ_{max}) for each vertebral joint, the hypural bones and four equally spaced segments of the caudal fin rays. Analysis of variance revealed pervasive significant effects of both swimming speed and longitudinal location on variables describing amplitude, phase and wavelength. The amplitudes of z_{max}, β_{max} and θ_{max} generally increased in a non-linear fashion from approximately 25 %L to the tip of the caudal fin, and the greatest speed-related increases occurred between 0.7 and 1.6 $L\,s^{-1}$. For the snout, the first caudal vertebra and the trailing edge of the caudal fin, mean values of z_{max} increased with speed from 0.004 to 0.012 L, from 0.005 to 0.012 L and from 0.053 to 0.066 L, respectively. For joints between the skull and the first vertebra, between the trunk and the tail vertebrae, and among the most posterior caudal vertebrae, mean values of β_{max} increased with speed from 1.2 to 1.7 °, from 0.6 to 0.9 ° and from 1.4 to 2.2 °, respectively. Within each swimming speed, values of β_{max} of the distal caudal fin commonly exceeded twice those of the proximal caudal fin. Surprisingly, at a given longitudinal location, the times of maximum lateral displacement and bending did not occur simultaneously. Instead, the phase of z_{max} relative to β_{max} was commonly shifted by more than one-sixth of a cycle. Furthermore, the phase shift between z_{max} and β_{max} changed significantly with increased swimming speed. Angles of attack of the tail structures changed periodically from negative to positive values. Maximum angles of attack of the distal caudal fin ranged from 5 to 17 °, changed significantly with swimming speed and were less than those of the hypural bones of the tail. Mean tail-beat frequency increased significantly from 2.0 to 4.2 Hz with increased swimming speed. Estimated speeds of wave propagation showed considerable longitudinal variation, and the ratio of swimming speed to posterior wave speed increased from 0.59 to 0.83 with increased swimming speed.

Key words: locomotion, fish, swimming, kinematics, largemouth bass, *Micropterus salmoides.*

Introduction

Undulation of the axial structures is the most general form of aquatic vertebrate locomotion. Consequently, many kinematic features of steady undulatory swimming have been well described for diverse groups of vertebrates (reviewed by Gray, 1968; Webb, 1975; Lindsey, 1978). Among different species and for different locomotor speeds within a single species, key features of undulatory swimming known to vary include the following: (1) the length of the body that is undulated, (2) the frequency of undulation, (3) the amplitude of lateral displacement, and (4) the length of the propulsive wave (Gray, 1968; Lindsey, 1978). Most attempts to relate these attributes of undulating organisms to their anatomy have concentrated on the distribution of external surface area (Webb, 1982, 1988). For the purposes of hydrodynamic modeling, external morphology and the parameters describing wave form and speed have generally been sufficient to make numerous predictions about the energetics and relative efficiency of different species, swimming speeds and wave forms (Videler and Wardle, 1978; Videler and Hess, 1984; Webb *et al.* 1984; Webb, 1988).

However, to clarify the functional basis of undulatory swimming performance, it is also desirable to determine how internal morphology is related to externally visible movement. One particularly important kinematic variable for relating internal morphology to locomotor function is lateral bending (flexion) because the strain of the skin and axial muscles and

the kinesis of the intervertebral joints are all proportional to lateral flexion. Furthermore, the mechanical behavior of these tissues is affected by both the amplitude and frequency of lateral flexion (Wainwright, 1983; Long, 1992; Rome *et al.* 1993). However, compared with other parameters of wave form, the extent and/or timing of lateral bending have been quantified for only a limited number of undulating species (Grillner and Kashin, 1976; Videler and Hess, 1984; Williams *et al.* 1989; van Leeuwen *et al.* 1990; Rome *et al.* 1988). With the exception of recent work (Jayne and Lauder, 1993), previous studies quantifying the lateral bending of swimming fish have generally used the radius of curvature without incorporating the direct anatomical measurements of the vertebral column and tail that would be required to estimate vertebral flexion. Hence, interpreting the available data on bending during the undulatory swimming of vertebrates is complicated by differences in external shape and numbers of vertebrae, lack of internal anatomical data and tremendous differences in the phylogenetic affinities of the taxa that have been studied.

This study on the midline kinematics of *Micropterus salmoides* during steady swimming is one of a series that we have performed on two species of centrarchid fishes to clarify the effects of morphological variation on locomotor function. Our two chosen centrarchid species have conspicuous differences in their external shape: *M. salmoides* has a rather generalized fusiform shape, whereas *Lepomis macrochirus* has a deep body which may exceed 40 % of the standard length of the fish (Jayne and Lauder, 1994). However, these two species have approximately equal numbers of vertebrae (Scott and Crossman, 1973; Mabee, 1993), which facilitates a paired comparison designed to isolate the effects of external shape on locomotor function and performance.

The present study had the following aims. First, for each fish, we used anatomical data on midline skeletal segment lengths (obtained from X-ray photographs of each fish) to partition a mathematical function representing the fish midline into discrete lengths. This allowed us to estimate chosen kinematic parameters for specific anatomical landmarks along the length of the fish. Second, for the reconstructed midline of the fish, we quantified (1) lateral bending, (2) lateral displacement and (3) orientation with respect to the overall direction of travel. Third, we quantified the timing of these three kinematic events to determine their rates of propagation. Fourth, we examined the phase relationships among these three kinematic events, which have not often been determined simultaneously for a single species. Fifth, we examined whether the above quantities and relationships varied significantly with swimming speed and among different longitudinal locations. We attempted to examine as large a number of anatomically defined longitudinal locations as possible to clarify events that occur along the entire length of the fish, and we employed a suitable experimental design to facilitate future comparisons with *Lepomis macrochirus* and other species with differing morphology.

Materials and methods

Experimental subjects and protocol

We obtained five *Micropterus salmoides* Lacépède (largemouth bass) from ponds in southern and central California. The bass were fed a maintenance diet of earthworms and goldfish, and their average time in captivity before experiments was approximately 3 months. All fish were maintained at a constant temperature of 20±2 °C, which was the same mean value as the water temperature used during experiments (20±0.5 °C). The larger individuals were housed individually in 84 l tanks, whereas the smaller individual was kept in a 42 l tank.

For four individuals, the average values (and range) of total length (*L*), standard length (*SL*) and mass were 24.5 cm (23.9–25.1 cm), 20.5 cm (20.1–21.0 cm) and 165 g (149–174 g), respectively, and for one individual, these quantities were 18.4 cm, 15.4 cm and 111 g. As far as possible, we attempted to use individual bass with masses that were similar to those of the bluegill (*Lepomis macrochirus*) used in a parallel series of experiments. The tail depth (*B*) of the fish averaged approximately 0.27 *L* and the greatest span across from the edges of the dorsal and anal fins approximated 0.29 *L*. For the range of swimming speeds which we observed, the bass did not fully erect either their soft dorsal or anal fins, and the average maximal vertical distance of this region of the fish was approximately 0.26 *L*. Using the method of Webb (1988), the wetted surface area of the large individuals and small individuals approximated 270 cm^2 and 145 cm^2, respectively. After some additional experiments, the fish were preserved and X-ray photographs were taken to determine the numbers and lengths of various axial skeletal structures, including the skull, the centra of individual vertebrae and the length of the ural+hypural bones of the tail.

We used a calibrated flow tank to obtain steady swimming from each the bass at average forward speeds of 0.7, 1.2, 1.6, 2.0 and 2.4 $L\,s^{-1}$. The working section of the flow tank was 18 cm×18 cm×46 cm, with the long dimension being parallel to the flow. Prior to the experiments, flow speeds were determined by videotaping dense clouds of Methylene Blue dye, which were injected at 2–3 cm intervals along the height and width of the working section, and then we generated calibration curves relating flow to the digital display of a tachometer that indicated the rotation speed of the propellor in the flow tank. We only analyzed sequences of fish that were swimming more than 3 cm away from the sides and bottom of the tank and below the surface of the water. Furthermore, we were nearly always successful in centering the fish in the flow tank, and the resulting gap span ratios (Webb, 1993) of the large and small fish approximated 1.2 and 1.6, respectively. We used strict criteria for selecting steady swimming. Sequences were only analyzed if the change in upstream–downstream position of the fish was less than 3 mm per tail beat. With the exception of the two fastest speeds, the change in upstream–downstream position was usually less than 3 mm

over the entire time interval analyzed. Consequently, the variation in forward swimming speed among different tail beats within each sequence was less than 5 %.

Image acquisition and analysis

We obtained video tapes of the swimming fish using a two-camera high-speed video system (NAC HSV-400) operating at 200 images s^{-1}. A front-surface mirror beneath the flow tank provided a direct ventral view to one camera, and the second camera obtained a lateral view. The lateral view was used primarily to ensure that the fish was centered between the surface of the water and the bottom of the flow tank. Most of the kinematic analysis was based on the ventral view of the fish, which was back-lit by two 500 W photoflood light bulbs. For each swimming speed, we analyzed an overall time interval which was slightly longer than four tail beats. Within each sequence, we selected video images spaced approximately 1/20 of a tail beat apart. The actual number of images analyzed per tail beat ranged from 16 to 23.

Fig. 1 summarizes the sequence of five key steps involving the custom-built software that we used for a frame-by-frame analysis of the ventral image of the swimming fish. (1) 25–30 points were digitized along both the left and the right sides of the fish (Fig. 1A). (2) A cubic spline function then used these coordinates to calculate the coordinates of 500 points used to construct a smooth outline of each side of the fish (Fig. 1B). (3) Using an iterative computer algorithm and the 1000 points constituting the reconstructed outline, the coordinates were determined for 30 points for which distances to the nearest left and right side outline points were equal (Fig. 1C). (4) For these 30 points, cubic spline functions were used to generate a smooth midline consisting of 500 points (Fig. 1D). (5) Starting from the most anterior location, cumulative distances were calculated for the reconstructed midline such that it was partitioned into pieces (Fig. 1E) whose lengths were equal to those of the axial skeletal structures described in more detail below.

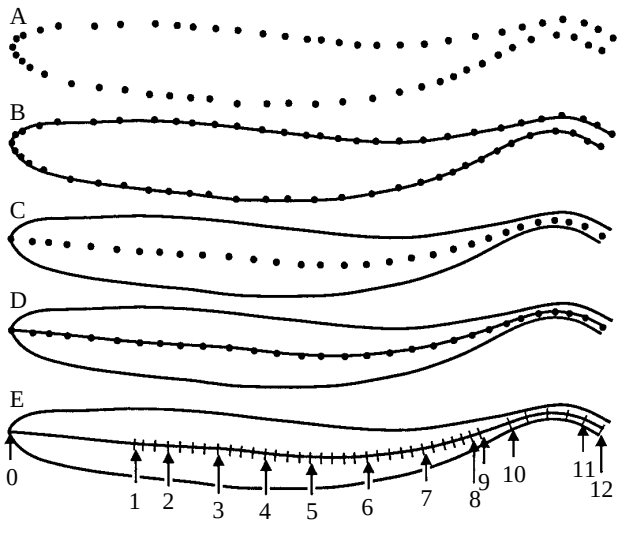

Fig. 1. Diagrammatic view showing the method for reconstructing the midline of fish. (A) The fish outline was digitized in each video field. (B) Cubic spline functions were fitted to both the right and left sides. (C) Using the outline cubic spline functions, 30 midline points were determined by an iterative computer algorithm. (D) Cubic spline functions were fitted to the 30 midline points. (E) The midline was partitioned into lengths of various axial structures determined from X-ray photographs. The numbers refer to the standardized anatomical locations used in statistical analyses (see Table 1).

The splines referred to in steps 2 and 4 (Fig. 1B,C) used cubic polynomials. The first cubic polynomial of the spline was fitted to points 1–6 (where point 1 is the most anterior), the second polynomial to points 2–7, etc. The equations for the polynomials were weighted such that where the two polynomials overlap (at point 2 for the first two polynomials) the region forms a continuous curve. In preliminary analyses, we overlaid the reconstructed outlines directly onto the video image to ensure that the choice of sampling intervals for the cubic spine resulted in reconstructions which closely matched the original image. Because the sides of fish, as seen in ventral (or dorsal) view, lack distinct landmarks that are strictly homologous, a technical problem analogous to that in morphometric studies of outline shapes that lack homologous landmarks arises. Hence, we chose a method for midline reconstruction which closely resembles the median axis method that has been used in morphometric studies of outline shapes (Straney, 1990) and has been shown to yield results comparable using various Fourier methods for shape analysis. Compared with the sides of an undulating fish, which continually change length, the bones of the axial skeleton have a relatively constant length. Thus, partitioning the midline into segments representing bone lengths provides a partial, but not perfect, solution to the difficult problem of analyzing silhouetted views of swimming fish that lack significant numbers of clearly recognizable homologous landmarks.

Following completion of the experiments, the fish were preserved and a high-resolution X-ray photograph obtained of each fish in lateral view (using a Hewlett-Packard Faxitron X-ray system). The lengths of each axial structure along the body of the bass were digitized from the X-ray photograph. Specifically, from the X-ray photograph of each fish, we measured the lengths of the skull, each vertebra and the hypural bones plus the supporting fused ural (tail) vertebrae. The flexible caudal fin rays were divided into five segments of equal length, and we used all of the resulting measurements to partition the reconstructed midlines (Fig. 1E). Hence, for each of the intersegmental joints along the midline, we generated files containing the x and z coordinates of the joints, and β, the angle between the two adjacent segments of each joint. The x and z coordinates of the endpoints of each midline segment were then used to calculate θ, the angle of orientation of an individual segment with respect to the overall direction of travel (Fig. 2B). To correct for the minor differences in size among the different individuals, all linear measurements were transformed to units of total length (L). Using data from the edge of the caudal fin (Fig. 1E, site 12), plots of z *versus* time were used to determine the duration (period) of each tail beat and the inverse of this quantity, f, the tail-beat frequency (in Hz).

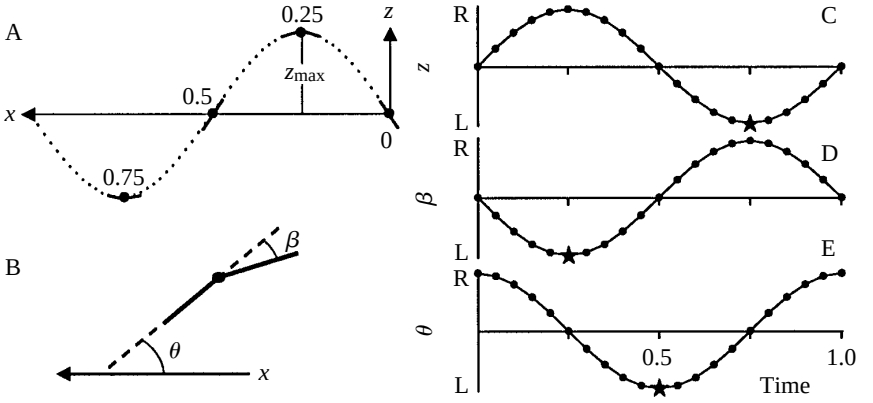

Fig. 2. Conventions for calculating kinematic variables and predictions for phase relationships among kinematic variables for a single longitudinal location assuming sinusoidal movement. (A) Orientation of axes. The thin dotted line represents the path traveled by a single longitudinal site, which is shown at four times (0 %, 25 %, 50 % and 75 % of the cycle duration). The overall direction of forward travel (parallel to the flow and long axis of the tank) is indicated by *x*. Lateral displacement and its amplitude are *z* and z_{max}, respectively. In A and B, the large dots represent the joints between two adjacent midline segments (thick lines). (B) For the illustrated hypothetical longitudinal site (between times 0.25 and 0.5 in A), both orientation (θ) and lateral flexion (β) are negative. (C–E) Plots of lateral displacement (C), lateral flexion (D) and orientation (E) *versus* time for a hypothetical longitudinal site that travels along and conforms to a sinusoidal path (as shown in A). R and L indicate right and left; units of *z* are cm and those for β and θ are degrees. Note that, when a site is maximally displaced to the right (time=0.25), one would expect that it would be maximally concave to the left. When the anterior end of the anterior axial structure is oriented to the right of the joint, θ is positive. Stars indicate landmark kinematic events whose elapsed times were used for calculations of phase and phase shifts.

Fig. 2 describes the conventions used for orienting the coordinate axes and for determining the signs of our kinematic variables. Negative values of *z*, β and θ indicate displacement to left, lateral flexion concave to the left and orientation to the left, respectively. We imported data on these three kinematic variables (*z*, β and θ) into a graphics program, which we used to digitize the maximum and minimum values and the elapsed times at which these landmark events occurred. For each cycle, we determined three amplitude variables (z_{max}, β_{max} and θ_{max}) as half of the mean difference between two successive maxima and minima (spaced at intervals of half the period of the tail beat). Thus, during one cycle, values oscillate from positive to negative values of z_{max}, β_{max} and θ_{max}. Within each of three quantities (*z*, β and θ), we determined the difference in the elapsed times of the landmark events (Fig. 2C–E) at each longitudinal site relative to site 11 (Fig. 1E) and then divided the result by the period in order to calculate the phase of each longitudinal location. We calculated three additional variables (*z*–β shift, *z*–θ shift and β–θ shift) describing the phase shift of one kinematic variable with respect to another kinematic variable. Hence, all values of phase and phase shift variables indicate a proportion of a period (i.e. 1=cycle duration). If the body of the fish traveled along a sinusoidal path, and its body conformed perfectly to the path traveled, then one would expect a site to be maximally concave to the left when it is maximally displaced to the right (Fig. 2). For these conditions, the values of *z*–β shift, *z*–θ shift and β–θ shift would be (±)0.5, 0.25 and −0.25, respectively, and these were our *a priori* expectations for the phase shifts among pairs of variables at each and every longitudinal site (compare positions of star markers in Fig. 2C,D,E).

Statistical analysis

To reduce the data set for statistical analysis, we defined 13 standardized longitudinal positions (see Fig. 1E and Table 1). Individual fish differed slightly in their numbers of vertebrae; hence, the midlines were not always partitioned into equal numbers of segments for all individuals. In order to compare anatomically similar locations among different individuals, for sites 2–7 (Table 1), we chose locations spaced at equal numbers of vertebrae proceeding either anteriorly or posteriorly from the joint between the trunk and caudal vertebrae (site 5). Additional sites included the most anterior and posterior extents of the vertebral column, the specialized bones (ural vertebrae+hypurals) intrinsic to the tail, and the distal two-fifths of the caudal fin. Changes in *z* with time were sufficiently large so that periodic variation in *z* could be detected along the entire length of the fish, and hence z_{max} and *z* phase were determined for all 13 sites (Table 1). Because the opercula obscured the view of trunk flexion anterior to site 3 and because only small amounts of lateral bending occurred anterior to site 4, measurements of β and β phase were only analyzed statistically for sites 4–11. We were primarily interested in θ because of its importance for trailing-edge kinematics (site 12), but we included a few additional sites to allow some calculations of the rates of propagation and phase shifts with respect to other kinematic variables.

Our primary statistical analysis was a three-way mixed-model analysis of variance (ANOVA) with speed (*N*=5), site (see Table 1 for *N* values) and individual (*N*=5) as the three main effects. We considered speed and site as fixed factors and individual as a random factor, and we followed the guidelines given by Zar (1984) for performing *F*-tests. In this model, the mean squares of speed and site were divided by their respective two-way interaction terms with individual in order to calculate the *F*-value. We used the GLM procedure of SAS version 6.07 to calculate the type III sums of squares, which were used in the ANOVA. For each individual at each speed, we had three or four observations for all variables involving *z*, β and θ. Thus, the different numbers of sites and minor differences in the numbers of observations per cell of our experimental

Table 1. *Summary of standardized longitudinal positions of the anatomical sites of interest of the five* Micropterus salmoides *used for statistical analysis of the kinematics (see also Fig. 1)*

Site number	Variables measured	Mean (L)	Individual					Description
			1	2	3	4	5	
0	z	0	0	0	0	0	0	Tip of snout
1	z, θ	0.214	1	1	1	1	1	Joint between skull and first vertebra
2	z	0.270	4	5	4	4	4	Twelve joints anterior to site 5
3	z	0.352	8	9	8	8	8	Eight joints anterior to site 5
4	z, β	0.430	12	13	12	12	12	Four joints anterior to site 5
5	z, β, θ	0.505	16	17	16	16	16	Joint between trunk and tail
6	z, β	0.596	21	22	21	21	21	Five joints posterior to site 5
7	z, β, θ	0.686	26	27	26	26	26	Ten joints posterior to site 5
8	z, β	0.769	31	33	31	31	30	Most posterior intervertebral joint (includes preural vertebrae)
9	z, β	0.784	32	34	32	32	31	Preural–hypural joint
10	z, β, θ	0.833	33	35	33	33	32	Hypural–tail fin joint
11	z, β, θ	0.967	37	39	37	37	36	20 % tail fin length anterior to tip
12	z, θ	1.000	38	40	38	38	37	Posterior tip of tail fin

The number of midline 'joints' (Fig. 1E) posterior to the skull for each site is given below each individual.
Mean L indicates the average (N=5) distance of the site from the snout measured in total lengths.
For the variables indicated at the left, maximal values were determined as well as their phase with respect to site 11.

Table 2. *Summary of* F*-values from ANOVAs of kinematic variables*

Kinematic variable	Main effects			Interactions			
	Speed	Site	Individual	Speed × individual	Site × individual	Speed × site	Speed × site × individual
z_{max}	13.2** (4, 16)	478.7** (12, 48)	63.4** (4,900)	14.6** (16, 900)	2.6** (48, 900)	4.0** (48, 192)	1.3 (192, 900)
β_{max}	9.0** (4, 16)	153.0** (7, 28)	14.1** (4, 579)	5.9** (16, 579)	17.4** (28, 579)	4.7** (28, 112)	2.4** (112, 579)
θ_{max}	27.7** (4, 16)	1161.2** (5, 20)	46.4** (4, 434)	7.1** (16, 434)	4.6** (20, 434)	8.5** (20, 80)	1.4 (80, 434)
z phase	5.5* (4, 16)	1255.9** (12, 48)	161.3** (4, 948)	27.6** (16, 948)	8.1** (48, 948)	5.2** (48, 192)	1.5** (192, 948)
β phase	7.0* (4, 16)	409.8** (7, 28)	36.9** (4, 584)	8.4** (16, 584)	8.3** (28, 584)	7.3** (28, 112)	1.3 (112, 584)
θ phase	15.6** (4, 16)	1294.4** (5, 20)	22.8** (4, 438)	3.2** (16, 438)	5.5** (20, 438)	6.7** (20, 80)	1.5* (80, 438)
z–β shift	5.1* (4, 16)	2.9 (7, 28)	17.9** (4, 584)	11.1** (16, 584)	5.8** (28, 584)	4.4** (28, 112)	1.4* (112, 584)
z–θ shift	2.0 (4, 16)	107.5** (5, 20)	46.0** (4, 438)	30.0** (16, 438)	2.5** (20, 438)	1.5** (20, 80)	1.9** (80, 438)
β–θ shift	0.5 (4, 16)	3.5 (3, 12)	12.5** (4, 292)	8.6** (16, 292)	6** (12, 292)	7.6** (12, 48)	1.5 (48, 292)
f	46.1** (4, 16)		43.2** (4, 54)	11.3** (16, 54)			
L period^{-1}	27.9** (4, 16)		34.8** (4, 54)	7.7** (16, 54)			

The degrees of freedom are indicated in parentheses below each F-value.
See Materials and methods for further details.
*$P \leqslant 0.005$; **$P < 0.001$.

design were responsible for the variable degrees of freedom associated with the F-tests listed in Table 2.

To provide descriptive statistics for some of the longitudinal locations not included in the ANOVAs, we used data from

individual 2 (Table 1), which generally had mean values that were intermediate to those of the other individuals. We also used individual 2 to determine variation in trailing-edge height and to perform some additional calculations including the angle of attack (α). Tukey *post hoc* comparisons revealed that values for the smallest fish were commonly not significantly different from values for all of the other individuals; therefore, we simultaneously analyzed the data from all five individuals which spanned the size range of the *Lepomis macrochirus* that were used in a parallel set of experiments to be reported elsewhere.

Because multiple ANOVAs were conducted on 11 different variables (Table 2), we used the 0.005 probability level as our criterion for statistical significance.

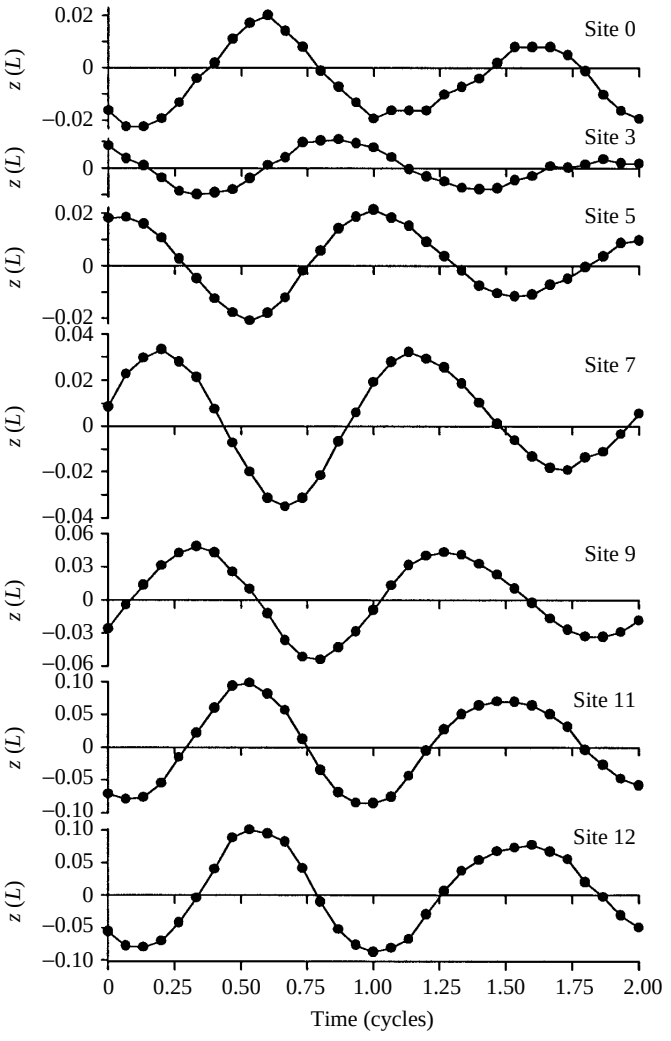

Fig. 3. Plots of lateral displacement, *z*, *versus* time for 0.8 s of swimming at $1.6L\,s^{-1}$ by a single individual with L=24.5 cm. The locations of the different longitudinal sites are as given for individual 2 in Table 1. Note also that the scale of the ordinate is the same for only the top four graphs. Note the posterior propagation of the wave crest which takes about one period to pass from the snout (top) to the tip of the tail (bottom).

Results

Amplitude variables

Lateral displacement (z), lateral flexion (β) and orientation angles (θ) all varied in a more or less sinusoidal pattern with time (Figs 3, 4). Thus, the amplitudes (z_{max}, β_{max} and θ_{max}) of each of these quantities were calculated as half of the difference between each successive minimum and maximum. All main effect terms of the three-way ANOVAs were highly significant for z_{max}, β_{max} and θ_{max} (Table 2); hence, amplitudes varied significantly among different swimming speeds, among longitudinal locations along the midline and among different individuals. Even when the amplitude variables were re-analyzed using data only from longitudinal locations within the vertebral column (Fig. 1E, sites 2–8), all main effects of the three-way ANOVAs were still highly significant.

Fig. 5 shows the mean values of each longitudinal location for each of the five swimming speeds studied. The most pronounced changes in amplitudes were the increases that occurred with increased swimming speed from 0.7 to $1.6L\,s^{-1}$. For example, between 0.7 and $1.6L\,s^{-1}$, mean values of z_{max} for the tip of the snout (site 0), the intervertebral joint between the trunk and tail (site 5) and the most posterior intervertebral joint (site 8) increased from 0.004 to $0.012L$, from 0.005 to $0.012L$ and from 0.018 to $0.033L$, respectively. Over the same speed range, mean β_{max} at sites 5 and 8 increased from 0.6 to 0.9° and from 1.4 to 2.1°, respectively. Between 0.7 and $1.6L\,s^{-1}$, mean values of θ_{max} of the skull increased markedly from 0.6 to 2.7°,

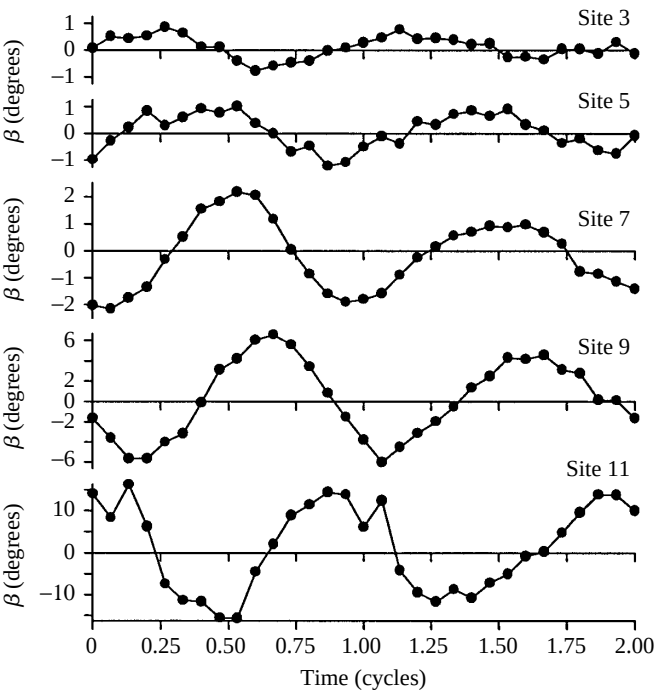

Fig. 4. Plots of lateral flexion, β, *versus* time for the same individual and time interval as shown in Fig. 3. The scale of the ordinate is the same for only the top three graphs. Note the posterior propagation of lateral bending.

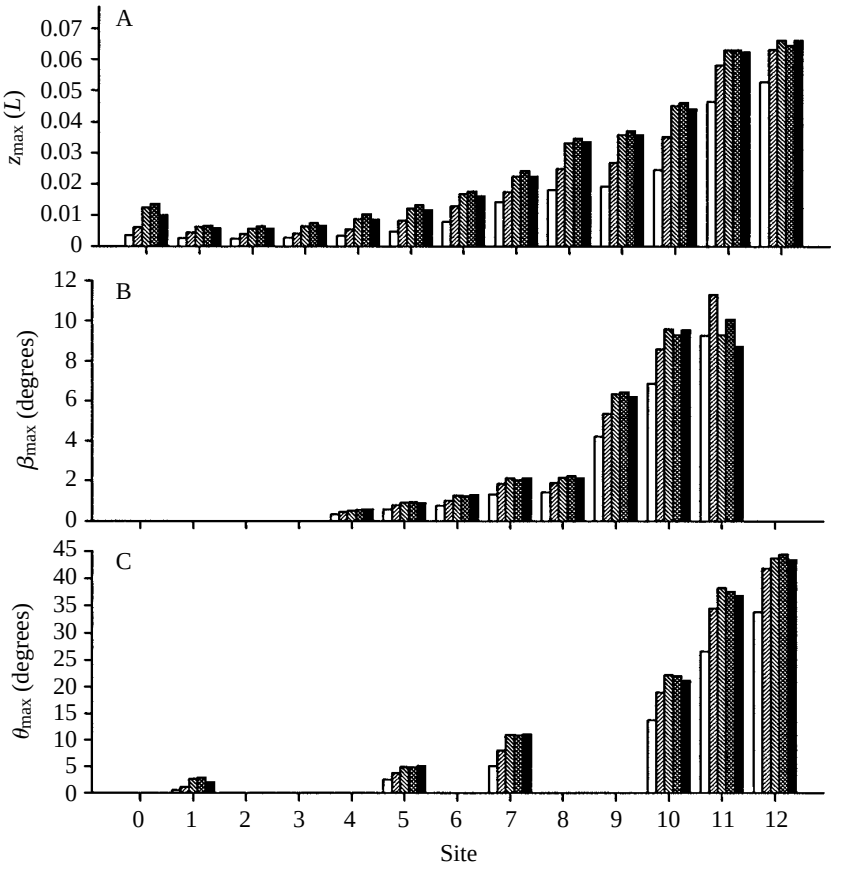

Fig. 5. Mean values for the amplitudes of lateral displacement (A), lateral flexion (B) and orientation (C). Data were pooled for all observations of all five individuals and, for each longitudinal site (Fig. 1E), means are arranged from the lowest (white) to the highest (black) swimming speed (0.7, 1.2, 1.6, 2.0 and $2.4\,L\,s^{-1}$). See Table 2 for significance levels. Note that the distance along the *x*-axis does *not* indicate the distance from the snout of the fish (see Table 1 and Fig. 1E for mean longitudinal positions of the sites).

while mean values of θ_{max} at site 5 had a smaller relative increase from 2.5 to 4.8°.

Further increases in swimming speed (from 1.6 to $2.4\,L\,s^{-1}$) were accompanied by little, if any, change in the mean values of the amplitude variables. For example, for the cumulative amplitude data shown in Fig. 5, 25 of 27 comparisons (among speeds within sites) between values at 1.6 and $2.4\,L\,s^{-1}$ had relative changes of less than 10 %. The two mean values of amplitudes with the greatest changes between 1.6 and $2.4\,L\,s^{-1}$ were for variables describing movements of the snout and skull. Between 1.6 and $2.4\,L\,s^{-1}$, mean z_{max} of the snout decreased from 0.012 to $0.010\,L$ and mean θ_{max} of the skull decreased from 2.7 to 2.0°.

Fig. 5 also shows that at each of the five swimming speeds mean amplitudes varied considerably with the longitudinal location along the midline of the fish. Figs 6 and 7 show longitudinal changes in amplitude in greater detail by including longitudinal locations intermediate to the standardized locations that were used in the statistical analysis (Table 2; Fig. 5).

Minimal lateral displacement occurred at an intermediate longitudinal location approximately five vertebrae posterior to the skull ($0.27\,L$, Fig. 6A). Within each swimming speed, the amplitude of lateral displacement did not change longitudinally in either a simple linear or a simple curvilinear fashion (Fig. 6A). For all swimming speeds, the greatest rates of longitudinal change (slope of Fig. 6A) in the amplitude of lateral oscillation occurred within the proximal two-fifths of the caudal fin. However, the two slowest speeds differed from the other speeds in that their slopes (Fig. 6A) increased abruptly near $0.72\,L$. The data shown in Fig. 6 are from an individual (2 in Table 1) which had two pre-ural vertebrae anterior to the relatively large plate-like hypural bones of the tail, and the most anterior pre-ural vertebra was located very near to $0.72\,L$. Hence, at the slowest speeds, lateral oscillation of the tail fin and specialized tail bones are somewhat distinct from those of more anterior vertebral locations.

Fig. 6B shows the mean amounts of lateral flexion, β_{max}, for all the longitudinal locations along the midline of a single individual. At the joint between the skull and the first vertebra, values of β_{max} generally exceeded those of the intervertebral joints immediately posterior to them. Within each speed, β_{max} generally increased posteriorly along the vertebral column. Values of β_{max} increased abruptly at the joint between the hypurals and the pre-ural vertebra ($0.77\,L$). The increased values of β_{max} are partly a consequence of partitioning the most posterior portion of the midline into line segments that were longer than the lengths of vertebrae (approximately $0.02\,L$) that were used to partition the more anterior portions of the midline. However, the midline of the caudal fin was partitioned into five equal lengths (approximately $0.034\,L$). Thus, the amounts of lateral bending within the caudal fin are directly comparable with each other. Within each speed, the distal caudal fin commonly had more than twice the amount of

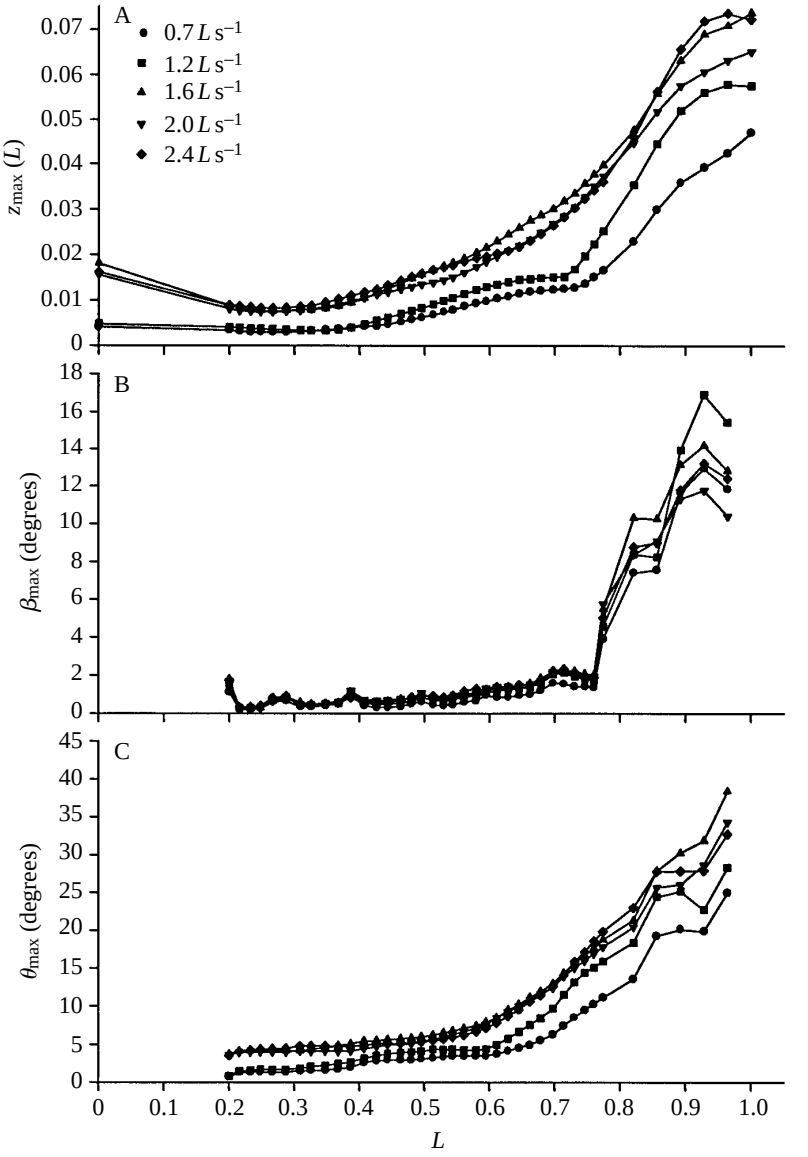

Fig. 6. Mean values for the amplitudes of lateral displacement (A), lateral flexion (B) and midline orientation (C) for all of the midline structures (skull, vertebrae, hypural bones and caudal fin divided into five parts) *versus* distance along the midline that the structure was positioned posterior to the snout. Data are for all tail beats (N=4) observed at all five speeds for a single individual (2 in Table 1) (L=24.5 cm).

lateral flexion of the proximal portion of the caudal fin (0.89 L, Fig. 6B).

Fig. 6C shows the mean values of the midline orientation relative to the overall direction of travel (θ_{max}) for all the longitudinal locations along the midline of a single individual. Similar to z_{max} and β_{max}, θ_{max} generally increased posteriorly. Unlike z_{max} and β_{max}, the minimum value of θ_{max} invariably occurred for the midline segment representing the skull (Fig. 6C, near 0.20 L). Values of θ_{max} showed a steeper rate of increase for the ten most caudal vertebrae ($0.60<L<0.75$) compared with more anterior locations within the vertebral column. Within each of the five speeds, values of θ_{max} of the hypural bones (0.82 L) were distinctly less than those of the proximal one-fifth of the caudal fin (0.86 L), whereas values of θ_{max} among the three most proximal caudal fin locations (0.86–0.93 L) were often quite similar to each other. The distal one-fifth of the caudal fin (0.96 L) always had the greatest values of θ_{max} within each of the five swimming speeds.

Timing variables

Within each tail-beat cycle for each individual, the times of z_{max}, β_{max} and θ_{max} at each site were converted to values of phase relative to site 11. The three-way ANOVAs revealed that all three phase variables (z phase, β phase and θ phase in Table 2) had highly significant variation among different longitudinal locations (as would be expected for a traveling wave). Somewhat unexpectedly, swimming speed significantly affected z phase and β phase, and the effects of speed on θ phase were highly significant. Fig. 7 shows the mean values for data pooled across all observations of all individuals at each longitudinal site. At a single longitudinal location, where significant differences were found among different speeds, the mean values of phase generally decreased in magnitude with increased swimming speed (Fig. 7). It is important to note that the standardized longitudinal locations were not equal distances apart (Table 1); hence, little difference in phase is apparent between closely spaced sites such as 8 and 9 (Fig. 7).

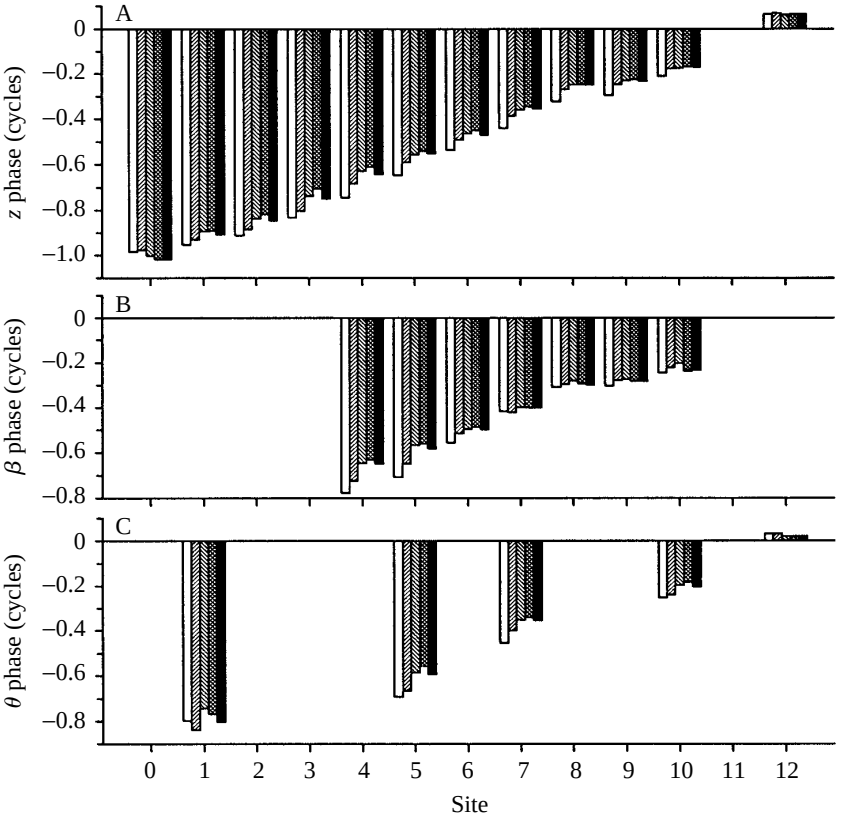

Fig. 7. Mean values for the phase of landmark kinematic events (see Fig. 2) with respect to site 11. Note that negative values indicate that an event at that site precedes that at site 11. Symbols and sample sizes are as in Fig. 5. (A). Lateral displacement. (B) Lateral flexion. (C) Orientation.

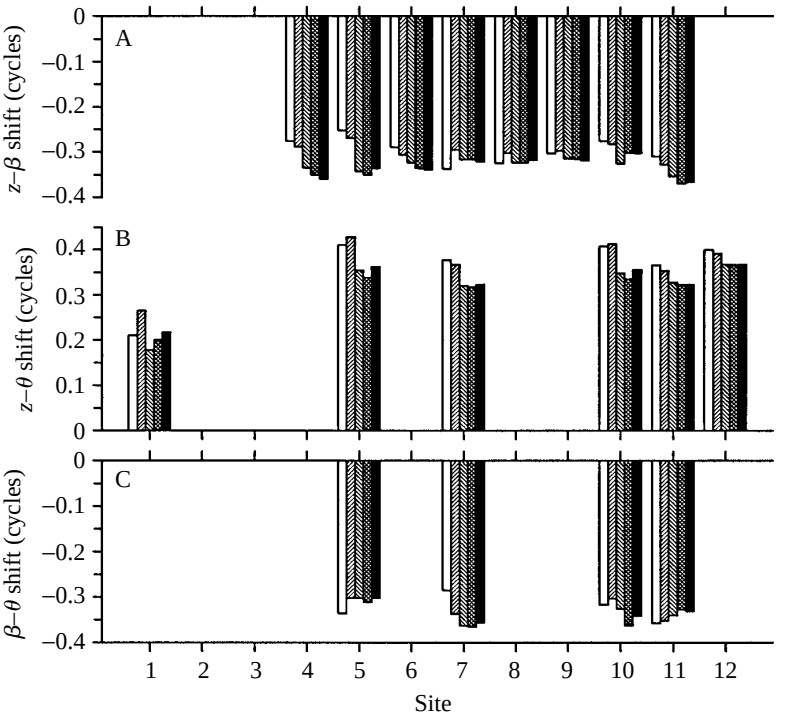

Fig. 8. Mean values for phase shift among the landmark kinematic events for pairs of different variables at each longitudinal site. Symbols and sample sizes are as in Fig. 5. (A) Phase shift between maximal lateral displacement and maximal lateral flexion. (B) Phase shift between lateral displacement and orientation. (C) Phase shift between lateral flexion and orientation. Values indicate the proportion of a cycle by which the former event lags behind the latter event of each pair.

At each longitudinal location, we also calculated the phase shift (Fig. 2C–E) between different kinematic variables (z_{max}, β_{max} and θ_{max}), and Fig. 8 shows the mean values for each of these phase shift variables (Table 2, z–β shift, z–θ shift and β–θ shift). None of the phase shift variables (Fig. 8) conformed to our *a priori* expectations (Fig. 2C–E) that z–β shift, z–θ shift and β–θ shift would have values of (±)0.5, 0.25 and −0.25 cycles, respectively. The mean values of z–β shift for each site at each speed ranged from −0.25 to −0.37 cycles (Fig. 8A). Consequently, z–β shift deviated substantially (0.25–0.13

cycles) from the expected value (−0.5 cycles). Negative values of z–β shift indicate that z_{max} preceded β_{max}. Excluding values for the skull, mean z–θ shift ranged from 0.32 to 0.43 cycles (Fig. 8B), indicating that z_{max} lagged slightly behind (0.07–0.18 cycles) θ_{max} compared with the prediction. The mean values of β–θ shift ranged from −0.37 to −0.29 cycles (Fig. 8C); therefore, β_{max} occurred slightly (0.13–0.04 cycles) earlier than expected relative to θ_{max}. For the sites included in the three-way ANOVA, the β–θ shift did not vary significantly either with longitudinal location or with swimming speed (Table 2). Values of z–θ shift were not significantly affected by speed, but there was highly significant variation among longitudinal sites, primarily as a result of the low values measured for the skull (Fig. 8B).

Surprisingly, the three-way ANOVA (Table 2) revealed that z–β shift changed significantly with speed (P=0.005), while the longitudinal position effect approached significance (P=0.025). Furthermore, z–β shift also had a highly significant speed by site interaction term (Table 2). Fig. 8A shows that speed did not conspicuously affect z–β shift at sites 7–9. However, at more anterior (sites 1–6) and more posterior (site 9 and above) locations (Fig. 8A), z–β shift increased significantly with decreased swimming speed such that values at the slowest speeds deviated most from the expected value of the z–β shift. Hence, maximum lateral displacement and maximum lateral flexion are not in phase, and their phase relationship changes significantly with swimming speed. Measurements of lateral displacement of undulatory swimmers have often been given without accompanying measurements of lateral bending (which is proportional to muscle strain). However, our results emphasize that it may be inadvisable to use the time of maximum lateral displacement as a surrogate measure for the time of maximal lateral bending in electromyographic studies of undulatory swimming (e.g. Frolich and Biewener, 1992).

The frequency of undulation, f (in Hz), changed significantly (Table 2) with swimming speed, u (in $L\,s^{-1}$), and this relationship was adequately described by the linear regression (using data in Fig. 9A): f=0.990+1.28u (r^2=0.85; P<0.001). The quantity u/f changed significantly with speed (Fig. 9B), and this indication of the distance traveled per period (in L) is analogous to the stride length of limbed animals. The coefficients of both the linear (P=0.001) and quadratic (P=0.019) terms were significant in the multiple regression equation (using data in Fig. 9B): u/f=0.137+0.381u−0.0811u^2 (multiple r^2=0.76), indicating that u/f differed little among the three highest relative swimming speeds.

Tail kinematics

Because of the importance of the tail in producing thrust, we performed a more detailed analysis of the kinematics of the tail including the hypural bones and the distal one-fifth of the caudal fin using four tail beats for each of the five swimming speeds of a single individual (2 in Table 1; L=24.5 cm). We used a one-way ANOVA to test for significant effects of speed and a Tukey *post hoc* test to compare group means of these data.

Fig. 10 shows the lateral displacement (z), orientation (θ),

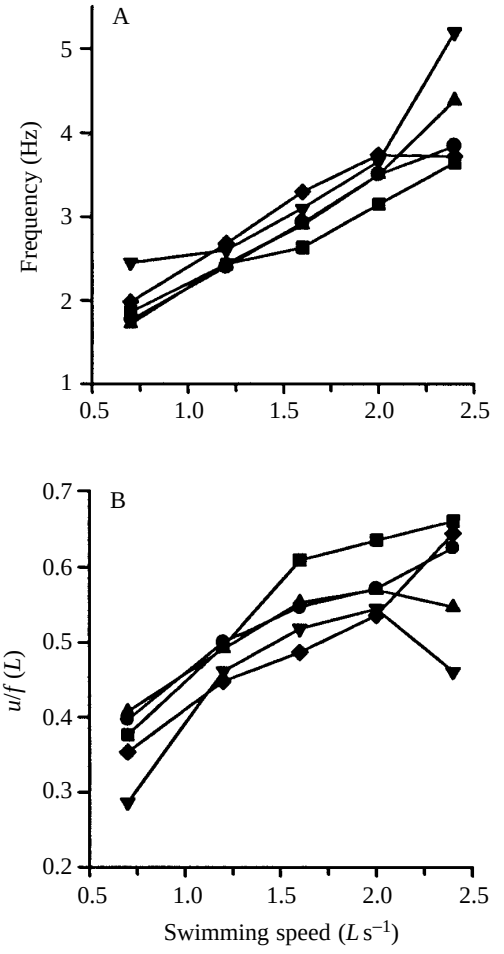

Fig. 9. Mean values of tail-beat frequency (A) and distance traveled per tail beat (B) *versus* forward swimming speed. Different symbols indicate different individuals. The diamonds indicate the values for the smallest fish, individual 5 (L=18.4 cm).

path angle and angle of attack (α) of portions of the tail for approximately two cycles of swimming at 2.4 $L\,s^{-1}$. Path angle represents the angle of the segment trajectory with respect to the overall direction of travel. Fig. 10 also illustrates the orientation of different portions of the tail relative to the paths traveled by the caudal midline segments. Fig. 11 clarifies that our positive values of α indicate that the lift vector contributed to thrust.

For both the hypurals and distal fin, z, θ, path angle and α all showed a clear pattern of periodic variation with time; however, the period of α (Fig. 10D,H) was half that of the other three kinematic variables (Fig. 10A–C,E–G). We observed both positive and negative angles of attack for the tail (Figs 10, 12) and, at a swimming speed of 2.4 $L\,s^{-1}$, the magnitude of α of the hypurals generally exceeded that of the distal fin (Fig. 10). Thus, the orientation (θ) of the distal fin more closely conformed to its path of travel than did that of the hypural bones at the base of the tail (Fig. 12A). Furthermore, at 2.4 $L\,s^{-1}$, α for the hypurals was positive for an average of 68 % of the cycle, whereas α was positive for

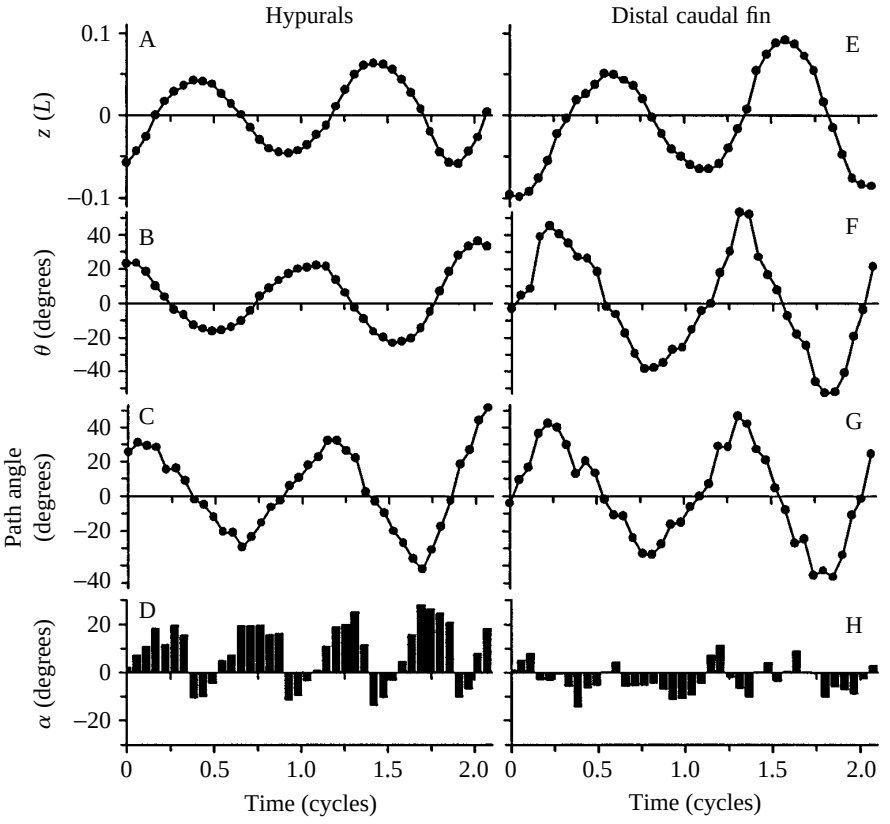

Fig. 10. Plots of lateral displacement, z (A,E), orientation, θ (B,F), path angle (C,G) and angle of attack, α (D,H), for the hypural midline segment (A–D) and the distal one-fifth of the caudal fin (E–F). Data are all from the identical 0.57 s of swimming at $2.4\,L\,s^{-1}$ by an individual fish (2 in Table 1) with L=24.5 cm. Positive values of the path angle indicate movement forwards and to the right. See Figs 2 and 11 for sign conventions of z, θ and α. Note that the ordinates of the plots of angles are all to the same scale.

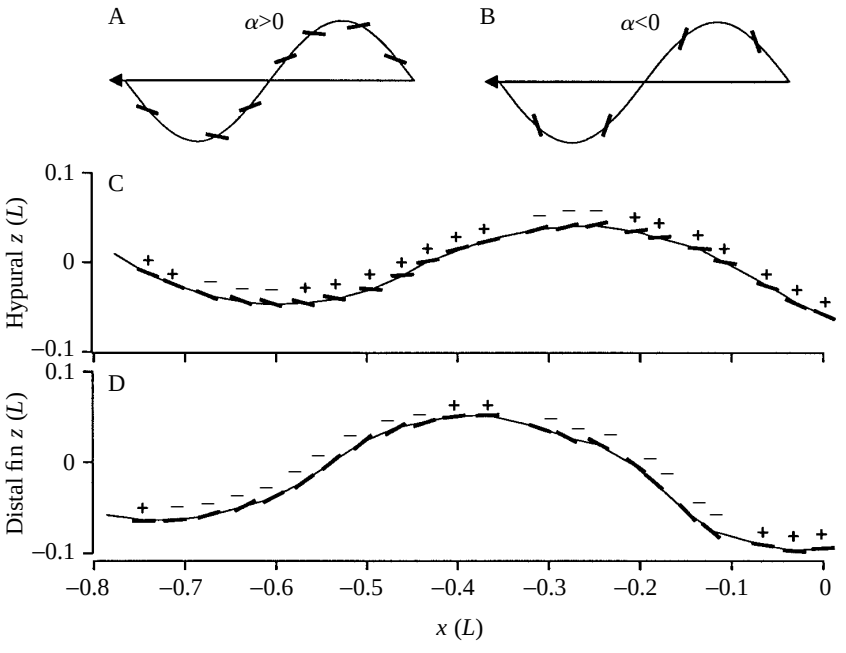

Fig. 11. Angles of attack, α, and the paths of midline segments as they travel from the right to the left. The sign conventions for α are shown in A and B for a hypothetical midline segment traveling along a sinusoidal path with an overall direction of travel indicated by the x-axis. Positive values of α indicate a lift vector with a forward-directed component which could contribute to thrust. Using the first 22 data points shown in Fig. 10 for individual 2 swimming at $2.4\,L\,s^{-1}$, the paths and orientations are shown for the hypural bones (C) and the distal one-fifth of the caudal fin (D) over the same time interval. In C and D, the path was determined for the midpoint of the midline segments and the experimentally observed values of θ were used to orient the thick lines relative to the path. The plus and minus signs above each midline segment in C and D indicate positive and negative values of α, respectively. The scales of the ordinate and abscissa are the same (C,D) in order to provide an undistorted view of the path traveled.

the distal fin for an average of only 41 % of a cycle. At all swimming speeds, values of α for both the hypurals and distal fin were simultaneously positive for only a small portion (approximately 10–20 %) of the tail-beat cycle, coinciding with the time when the trailing edge of the fin was maximally displaced laterally and when the hypurals were crossing the overall axis of travel (Figs 10, 11).

Swimming speed had widespread significant effects on the kinematics of the tail. Values of α_{max} for the hypurals varied significantly with speed ($F_{4,35}$=11.9; P<0.0001), with means (>20 °) at the slowest and fastest speeds which were almost twice as large as the three means at intermediate speeds (Fig. 12A). Values of α_{max} of the distal fin also varied significantly with speed (F=5.9; P=0.0009), the mean value at

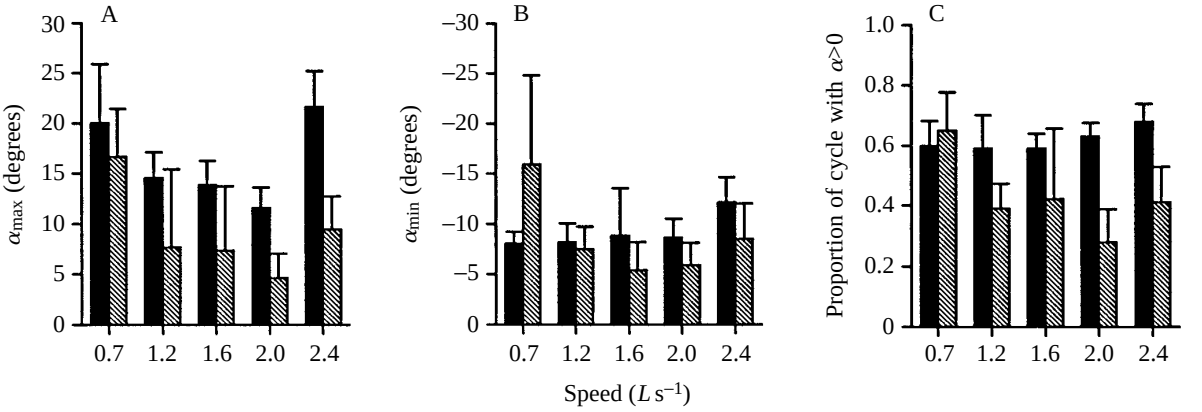

Fig. 12. Mean values (+ S.D.) of tail kinematic variables for four tail beats per speed for individual 2. N=8 for each mean in A and B, whereas N=4 for each mean in C. α_{max} and α_{min} indicate the maximum (positive) and minimum (negative) values (in degrees) observed for the hypurals and distal one-fifth of the tail fin for each half-cycle. (C) The proportion of each tail-beat cycle having positive α for the hypurals (filled columns) and distal tail fin (hatched columns). Data are for the same individual as in Figs 10, 11.

the slowest speed (16.7 °) being significantly greater than that at all other speeds (Fig. 12A). The greatest magnitude of the negative angles of attack of the hypurals (α_{min}) showed only marginally significant variation with speed (F=3.2; P=0.025), with the magnitude of the mean at the fastest speed (−12.1 °) being slightly greater than those at the slower speeds (Fig. 12B). Values of α_{min} for the distal fin varied significantly with speed (F=6.7; P=0.0004): the mean at the slowest speed (−16.7 °) had a greater magnitude than those at all faster speeds (Fig. 12B).

The proportion of the tail-beat cycle during which hypural α was positive (Fig. 12C) was effectively constant for all swimming speeds ($F_{4,15}$=1.1; P=0.36), having an overall mean value of 0.62 for all 20 observations. For the distal fin, the proportion of the cycle with positive α had marginally significant variation with speed (F=3.3; P=0.038) and this quantity tended to decrease with increasing speed (Fig. 12C). The combined changes in α_{min} and in the portion of each cycle with α>0 suggest that the kinematics of the distal fin may be most divergent from those of the hypurals at the fastest of the five swimming speeds observed in this study.

Waveform

The waveform of the midline of the undulating fish changed considerably as speed increased from 0.7 to 1.6 L s^{-1} (Fig. 13). For individual 2 (L=24.5 cm), wavelengths were determined as

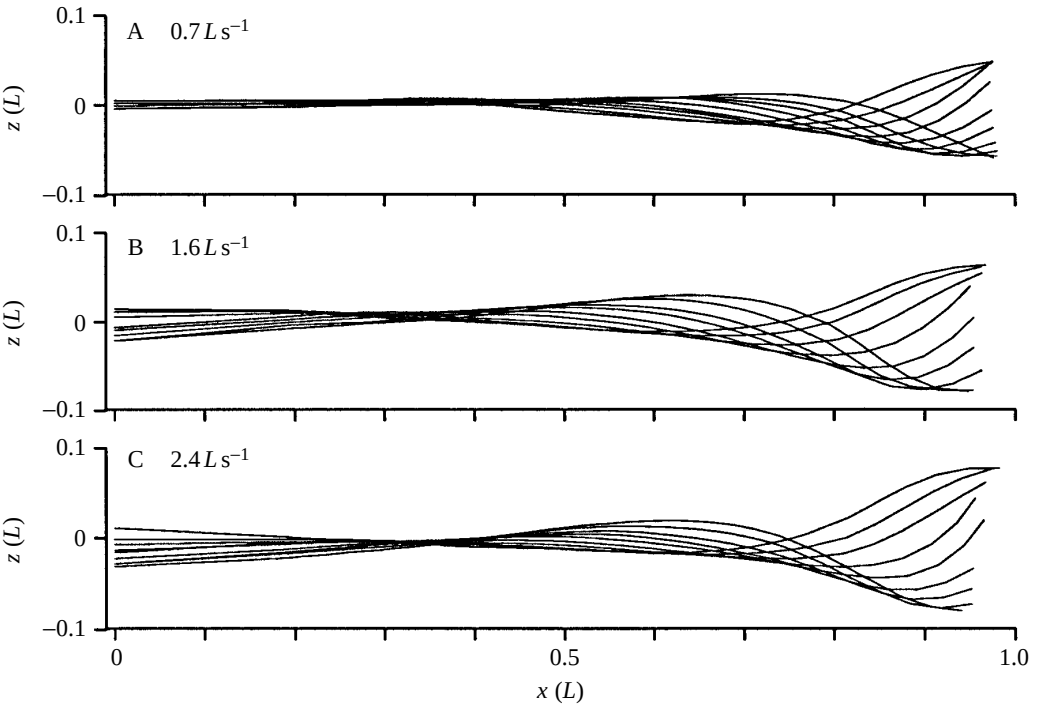

Fig. 13. Reconstructed midlines, superimposed after correcting for the forward displacement of a single swimming fish. Anterior is to the left in each figure. Successive midlines are spaced at equal time intervals (35, 25 and 15 ms for A, B and C, respectively) for approximately half a tail-beat cycle in each figure. The abscissa and ordinate are both to the same scale in order to provide an undistorted view. Note that the skull extends to approximately 0.2 L.

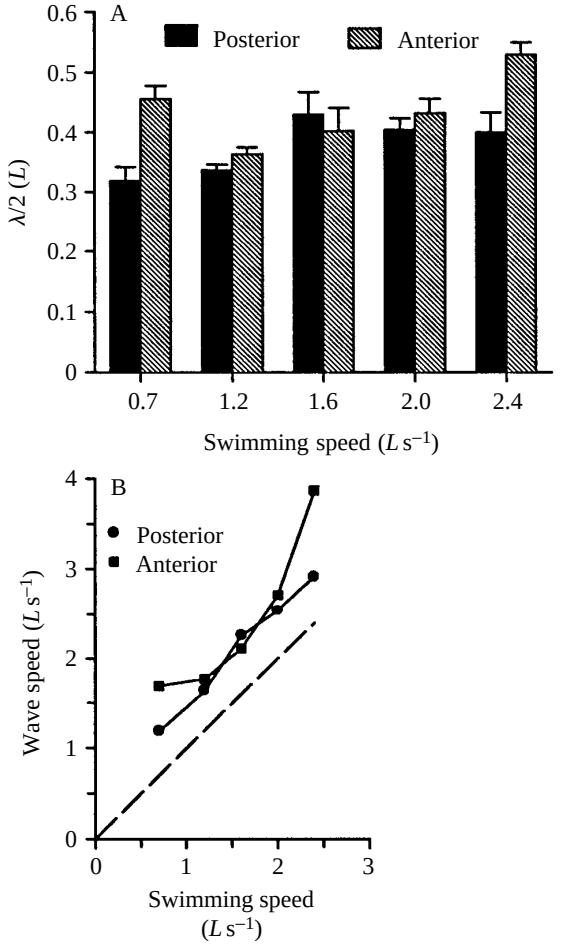

Fig. 14. (A) Mean + S.D. (N=4) internodal distances for individual 2 determined by superimposing pairs of reconstructed midlines which were 180° (or 0.5 cycles) out of phase. The anterior half-wave included a node at the first vertebra and extended posteriorly, whereas the posterior half-wave included the node at the tip of the caudal fin and extended anteriorly. (B) Mean wave speed (c) *versus* swimming speed (u) determined from the values shown in A multiplied by the mean tail-beat frequency for each of the five swimming speeds. The dashed line indicates a 1:1 ratio of c to u. For the posterior wave, the regression equation is c=1.04u+0.46 (N=5, r^2=0.98, P<0.001).

twice the internodal distances of superimposed midlines 0.5 cycles out of phase. Internodal distances were determined for two longitudinal locations. The anterior location included the half-wave with an internode at the first vertebra and proceeded posteriorly, whereas the posterior location included the half-wave with an internode at the trailing edge of the caudal fin and proceeded anteriorly. Using four observations at each of the five swimming speeds, a two-way ANOVA was used to test for significant effects of swimming speed and longitudinal position on wavelength, λ.

Swimming speed ($F_{4,30}$=22), longitudinal location ($F_{1,30}$=22) and the speed by location interaction term ($F_{4,30}$=16) all had highly significant (P<0.0001) effects on λ. Fig. 14A shows the mean values of internodal distances at the anterior and posterior locations for each of the different swimming speeds. In the posterior location, the smallest mean values of λ (0.64 L) occurred during the slowest swimming speed, and λ increased to approximately 0.86 L at 1.6 L s^{-1} and showed little change with speed from 1.6 to 2.4 L s^{-1}. Values of λ in the anterior region at both the slowest (λ=0.91 L) and fastest speeds (λ=1.06 L) considerably exceeded those of the posterior region (Fig. 14A), whereas at intermediate speeds the anterior and posterior wavelengths were quite similar (Fig. 14A).

The waveform of the midline differed from that of a simple sine function because the inflection points (straight regions) of the midline wave were not located either at the internodes or along the x-axis. Instead, when the tail was displaced to the right, the anterior inflection point was to the left of the posterior inflection point. Hence, line segments connecting the two midline inflection points for different images of the swimming fish displayed a periodic yawing motion rather than being always located on the axis of forward travel (as would be the case for a simpler sine wave).

Discussion

Wave speed

The speed of posterior propagation of the undulatory wave (c) can be estimated as $f\lambda$, and this quantity for the posterior region increased linearly with increased swimming speed (Fig. 14B). Anterior wave speed increased curvilinearly with swimming speed (Fig. 14) and both the linear (P=0.03) and quadratic (P=0.01) terms of specific swimming speed (L s^{-1}) in the regression c=2.57−1.94u+1.02u^2 (multiple r^2=0.99, N=5) were significant. However, because of longitudinal variation in λ, and because λ is a large proportion of midline length, the quantity $f\lambda$ is minimally useful for determining the extent to which wave speed varies along the length of the undulating fish.

Alternatively, wave speed in the x direction can be estimated by determining the midline distance between a pair of longitudinal sites (from Table 1, column 3) and dividing by the time lag in z_{max} between the pair of sites (Table 3). The resulting quantity, the speed of wave propagation along the length of the fish, would be the upper limit of possible wave speed along the x-axis and, because most of the fish midline forms a small angle relative to the x-axis, these two different wave speeds should be very similar. Within each of the swimming speeds, large discrepancies in wave speed are apparent among the different longitudinal locations used to track the propagation of maximum lateral displacement (Table 3).

The most anterior pair of sites used to estimate wave speed were the tip of the snout and the base of the skull and, with no exceptions, this region had the fastest speed of propagation (of z_{max}) compared with other longitudinal locations. For all practical purposes, the skull of *Micropterus salmoides* can be considered as a rigid structure with respect to locomotor function. Consequently, posterior propagation of the region of

Table 3. *Mean rates of propagation of* z_{max} *along the midline of* Micropterus salmoides *for pairs of longitudinal locations (a, b) at each of the five swimming speeds*

Site a	Site b	Speed of z_{max} propagation from a to b ($L\,s^{-1}$)				
		0.7	1.2	1.6	2.0	2.4
0	1	12.68	11.19	5.83	5.97	8.02
2	3	1.97	2.50	2.45	2.54	3.47
3	4	1.75	1.62	2.11	2.92	3.12
4	5	1.53	2.05	3.15	3.72	3.48
5	6	1.58	2.32	2.93	3.58	4.55
6	7	1.88	2.16	2.56	3.03	3.28
7	8	1.37	1.78	2.25	2.95	3.26
10	11	1.25	1.90	2.29	2.80	3.28
11	12	0.99	1.20	1.60	1.78	2.11
10	12	1.19	1.70	2.11	2.51	2.95

Speeds of propagation equal mean midline distances (Table 1) between sites divided by time lag.

Time lags between sites were calculated as the differences in mean values of phase (Fig. 7A) multiplied by the mean period (0.51, 0.40, 0.34, 0.28 and 0.24 s) for each of the five speeds.

maximum lateral displacement cannot be attributed to the propagation of a region of bending. Instead, the phase of z_{max} for the posterior part of the skull differs from that of the snout (Fig. 7A) because of the combined effects of lateral oscillation of the vertebral column and lateral flexion between the skull and the vertebrae. Thus, the perceived propagation of z_{max} along the skull emphasizes the potential errors in assuming that posteriorly propagated regions of maximal lateral displacement are a result of the propagation of a wave of bending.

In contrast to the skull, the post-cranial positions along the midline did indeed bend laterally; however, within each swimming speed there was still substantial variation in the speed of wave propagation among different post-cranial longitudinal locations. For example, at a swimming speed of $1.6\,L\,s^{-1}$, the estimated wave speed (Table 3) near the midbody ($3.15\,L\,s^{-1}$) was nearly 50 % greater than estimates for the tail ($2.11\,L\,s^{-1}$ from sites 10–12). Hydrodynamic studies of subcarangiform swimming of fishes generally calculate λ and wave speed of over a large longitudinal interval of the fish (often approaching $1.00\,L$), use $f\lambda$ to estimate wave speed at the trailing edge of the caudal fin and use some measure of wave speed relative to swimming speed to estimate efficiency (e.g. Webb *et al.* 1984). An interesting area for further study is the extent to which longitudinal variation in λ and wave speed may affect estimates of hydrodynamic efficiency.

Estimating muscle strain

The estimates of lateral vertebral flexion (β_{max}) can be converted to estimates of the per cent resting muscle length assuming that the superficial, longitudinally oriented fibers located at the widest part of the fish keep pace with the changing curvature of the fish. Estimated relative muscle length was calculated as the percentage of the ratio of the lateral to midline radii of curvature, which equals $100\{[CL/(2\sin\beta_{max}/2)]-W/2\}/[CL/(2\sin\beta_{max}/2)]$, where CL is the average length of the centra of a pair of vertebrae and W is the maximum body width at a particular intervertebral joint. Subtracting 100 % from the relative muscle length yields an estimate of muscle strain expressed as a percentage change from resting length.

Table 4. *Strain of superficial red muscle fibers for four speeds of steady swimming estimated from mean values of morphological measurements and* β_{max}

	Site 4	Site 5	Site 6	Site 7
Body width (L)	0.113 (0.009)	0.102 (0.008)	0.084 (0.008)	0.064 (0.008)
Centrum length (L)	0.0190 (0.0006)	0.0183 (0.0011)	0.0184 (0.0008)	0.0178 (0.0007)
$0.7\,L\,s^{-1}$				
β_{max} (degrees)	0.3 (0.05)	0.6 (0.14)	0.8 (0.20)	1.3 (0.41)
Strain (%)	1.7	2.8	3.0	4.1
$1.2\,L\,s^{-1}$				
β_{max} (degrees)	0.4 (0.07)	0.8 (0.22)	1.0 (0.41)	1.8 (0.49)
Strain (%)	2.3	3.8	4.0	5.7
$1.6\,L\,s^{-1}$				
β_{max} (degrees)	0.5 (0.07)	0.9 (0.07)	1.3 (0.17)	2.1 (0.67)
Strain (%)	2.6	4.4	5.2	6.6
$2.4\,L\,s^{-1}$				
β_{max} (degrees)	0.6 (0.11)	0.9 (0.13)	1.3 (0.10)	2.1 (0.65)
Strain (%)	3.0	4.3	5.2	6.6

Site indicates the longitudinal location as defined in Table 1.

Body width and centrum length are mean values (N=5).

Values of β_{max} are means of the mean values observed for each of the five individuals.

All values in parentheses are standard deviations (N=5).

Table 4 summarizes mean values of body width and vertebral centrum lengths, which were used to convert β_{max} to estimates of muscle strain at several longitudinal locations over the observed range of steady swimming speeds. Estimated strains varied from a minimum of ±1.7 % anteriorly at $0.7\,L\,s^{-1}$ to a maximum of ±6.6 % at the fastest swimming speeds. Within each steady swimming speed, posterior muscle strain was approximately 2.5 times greater than that of the most anterior site. At all longitudinal sites, as swimming speed increased from 0.7 to $1.6\,L\,s^{-1}$, estimated muscle strain increased by approximately 50 %. However, few differences in muscle strain were apparent among the three highest speeds of steady swimming.

Muscle strains have been estimated using similar calculations with radii of curvature (combined with select observations of sarcomere length in preserved specimens) both for scup *Stenotomus chrysops* (±1.6 % anteriorly to ±5.7 % posteriorly) and for carp *Cyprinus carpio* (+7.5 % posteriorly) swimming near the maximal speed possible using only red muscle activity (Rome *et al.* 1990, 1993). For the *Micropterus salmoides* in our study, $2.4\,L\,s^{-1}$ was near the maximal speed that could be attained before switching to the burst-and-glide mode of swimming, and this closely resembles the experimental conditions used for the other species in previous studies. Hence, despite numerous anatomical and phylogenetic differences, estimated muscle strains of *Micropterus salmoides* are extremely similar to the available values for other species swimming steadily at comparable speeds.

During escape behavior, red muscle strains may be as high 12 % and β_{max} may exceed 6 ° for *Lepomis macrochirus*, a centrarchid fish with a more specialized deep body shape than its close relative *Micropterus salmoides* (Jayne and Lauder, 1993). If red muscle were to keep pace with the changing curvature of a carp during the escape response, muscle strain would exceed 25 % (Rome and Sosnicki, 1991). Thus, it appears likely that values for muscle strain and vertebral flexion during maximal steady swimming of *Micropterus salmoides* are probably less than half those expected for maximal locomotor efforts.

Comparisons with previous studies

Micropterus salmoides showed a combination of frequency and amplitude modulation with increased swimming speed. Fish species that swim with lateral undulations almost universally increase tail-beat frequency as swimming speed increases (reviewed by Webb, 1975). Numerous studies have described longitudinal variation in lateral displacement similar to that in the present study in which there is a minimal value slightly posterior to the skull and a complicated pattern of posteriorly increasing values (Videler and Wardle, 1978; Videler and Hess, 1984; Webb, 1988).

Other than for the escape response of *Lepomis macrochirus* (Jayne and Lauder, 1993), no values of lateral vertebral flexion of swimming fishes are available for comparison with those determined in the present study of *Micropterus salmoides*. Despite the large number of kinematic studies on the undulatory swimming of vertebrates, the effects of vertebral number on the kinematics and performance of swimming remain poorly understood. For example, two species of anguilliform swimmers (snakes), which had a nearly twofold difference in the number of vertebrae present, did not show any detectable differences in waveform, while lateral vertebral flexion simultaneously showed nearly twofold interspecific variation (Jayne, 1988). Similar large differences in vertebral numbers can be found among fishes that swim in the subcarangiform mode. For example, the centrarchids (including *Micropterus salmoides* and *Lepomis macrochirus*) have less than half the number of vertebrae found in salmonids (Scott and Crossman, 1973).

The most detailed comparisons of the kinematics of *Micropterus salmoides* can be made with the rainbow trout (*Oncorhynchus mykiss*, formerly *Salmo gairdneri*), which resembles *Micropterus salmoides* by having a similar generalized fusiform shape and using subcarangiform swimming. Furthermore, the steady swimming of effectively identically sized rainbow trout (L=5–55 cm including an individual with L=24.9 cm) has been studied intensively over a similar range of strictly controlled steady swimming speeds (approximately $0.5–2.5\,L\,s^{-1}$) (Webb *et al.* 1984; Webb, 1988). We used water temperatures of 20 °C in our experiments, whereas those used of Webb *et al.* (1984) approximated 15 °C or were not reported (Webb, 1988).

Table 5 summarizes the kinematic and hydromechanical quantities for *Micropterus salmoides* and *Salmo gairdneri* of equal length (24.5 cm). Trailing edge depths, B, and wetted surface area, S, of *Micropterus salmoides* and *Salmo gairdneri* were 6.5 and 5.2 cm and 270 and 239 cm^2, respectively. Tail-beat amplitude, H, and propulsive wave length, λ, were independent of swimming speed for *Salmo gairdneri* (Webb *et al.* 1984), whereas we observed significant increases in both of these quantities for *Micropterus salmoides* with increased swimming speed (Table 5). Values of H and λ for *Salmo gairdneri* were generally larger than those for *Micropterus salmoides*. Tail-beat frequencies, f, of both species were very similar in their magnitude and pattern of increase with increased swimming speed (Table 5). For the three fastest swimming speeds, u, *Micropterus salmoides* and *Salmo gairdneri* had effectively identical speeds of wave propagation, c, whereas at the two slowest speeds *Salmo gairdneri* had values 20–30 % greater than those of *Micropterus salmoides*.

The quantity $(u+c)/2c$ has often been used previously (e.g. Lighthill, 1971; Videler and Wardle, 1978; Webb *et al.* 1984) as a method of estimating efficiency, and this quantity for *Micropterus salmoides* increased with increased swimming speed and exceeded the values for trout, with the greatest disparity being at the slower swimming speeds. Mean thrust power for trout and *Micropterus salmoides* were very similar, with *Micropterus salmoides* having slightly lower values at low speeds and slightly higher values at high speeds (Table 5). Similarly, the power coefficients for both species were similar over the entire range of swimming speeds. Froude efficiency,

Table 5. *Comparison of kinematic and hydromechanical variables for a bass and a rainbow trout with* L=*24.5 cm*

	Swimming speed, u (cm s^{-1})				
Variable	17.2	29.4	39.2	49.0	58.8
Bass *Micropterus salmoides*					
H (cm)	2.60	3.09	3.23	3.19	3.23
λ (cm)	15.6	16.5	21.1	19.8	19.6
f (Hz)	1.89	2.53	3.04	3.55	4.06
c (cm s^{-1})	29.4	41.7	64.0	70.4	79.6
$(u+c)/2c$	0.791	0.852	0.806	0.848	0.869
$\cos\theta_{max}$	0.831	0.744	0.722	0.714	0.725
$10^3 \times P$ (J s^{-1})	2.1063	6.9404	17.5733	24.5341	35.6237
C_p	0.0309	0.0202	0.0216	0.0154	0.0130
η_F	0.749	0.801	0.731	0.788	0.820
Trout *Salmo gairdneri* (*Oncorhynchus mykiss*)					
f (Hz)	2.00	2.58	3.04	3.50	3.96
c (cm s^{-1})	40.7	52.4	61.8	71.1	80.5
$(u+c)/2c$	0.711	0.780	0.817	0.844	0.865
$\cos\theta_{max}$	0.479	0.535	0.580	0.625	0.670
$10^3 \times P$ (J s^{-1})	2.4090	7.7379	13.8521	21.4316	30.3317
C_p	0.0400	0.0255	0.0192	0.0152	0.0125
η_F	0.396	0.590	0.685	0.751	0.799

See discussion for further details, including calculation of trailing edge depth (B), and wetted surface areas (S).

Trout λ=20.3 cm and H=3.84 cm at all speeds.

$H=2z_{max}$; $c=f\lambda$; $W=\pi fH/1.414$; $w=W[1-(u/c)]$; $M=\pi\rho B^2/4$.

$P=MWwu-0.5Muw^2/\cos\theta_{max}$; $C_p=P/(0.5\rho Su^3)$.

Terminology follows that of Webb (1992).

Trout values are from scaling regressions in Webb *et al.* (1984) and Webb (1988).

H, tail-beat amplitude; λ, length of propulsive wave; f, tail-beat frequency; c, wave speed; u, swimming velocity; W, maximum body width; w, the velocity give to the water; M, added mass per unit length; ρ, the density of water; B, tail depth; P, mechanical thrust power; C_p, power coefficient; η_F, Fronde efficiency; S, wetted surface area of fish.

η_F (as calculated by Webb, 1992) was most similar for *Micropterus salmoides* and trout at the highest swimming speed; with decreased swimming speed, values of η_F for *Micropterus salmoides* exceeded those for the trout by increased amounts (Table 5).

Two factors may partially account for these differences in η_F. First, at the slowest swimming speed, it was common for *Micropterus salmoides* to use pectoral fin movements to a variable extent together with axial undulation, and at present it is not feasible to estimate the contribution to thrust by these structures (Gibb *et al.* 1994, discuss difficulties in estimating pectoral thrust forces in a related species). Second, the combined span of the dorsal and anal fins of *Micropterus salmoides* was as much as 8 mm greater than that of the trailing edge. Recently refined hydrodynamic calculations (Webb, 1988, 1992) have attempted to account for the thrust generated by this more anterior region of the fish, which has a greater span than the trailing edge. In order to perform this correction, θ_{max} must be determined for the medial fins, but the body of *Micropterus salmoides* was too wide in this region for this quantity to be reliably assessed. Given the approximate nature of the preceding hydrodynamic calculations (Webb, 1988, 1992), it appears that despite the large differences in the numbers of vertebrae between these two taxa many features of their hydrodynamics appear to be extraordinarily similar.

Values of midline orientation, θ, are needed both to estimate mean thrust power and to calculate the angle of attack, α. For *Micropterus salmoides*, trailing edge values of θ_{max} approximated 34° at the slowest swimming speeds and increased to approximately 45° at the three fastest speeds. The values of θ_{max} for *Salmo gairdneri* differed substantially, with maximal values of 61° occurring at the slowest speed and decreasing to 48° at the fastest speed (Webb, 1988). For the tail fin of a rather large cod (L=42 cm), Videler and Wardle (1978; Fig. 6) found that θ_{max} varied from approximately 30 to 45°. For *Salmo gairdneri*, Webb (1988) reported that the maximal trailing edge angle (minimum of $\cos\theta$) and lateral displacement were synchronous. In contrast, these two quantities of *Micropterus salmoides* were out of phase by 0.35–0.4 cycles (Fig. 9B), representing a deviation from the trout values by 0.1–0.15 cycles.

For *Micropterus salmoides*, θ_{max} was determined for a limited portion (the distal one-fifth) of the caudal fin because the phase of θ_{max} varied considerably (by more than 0.2 cycles) along the length of the collective tail structures (hypurals and caudal fin). Webb (1988) did not explicitly state which portion of the tail was used to determine θ_{max}. However, if the entire tail fin were used, then this would tend to underestimate θ_{max} compared with our methods; hence, the actual difference between *Micropterus salmoides* and trout could be even larger than indicated above. Measurements of the phase between the trailing edge angle and lateral displacement can also be affected by the extent of the tail used to determine trailing edge angle.

For *Micropterus salmoides*, α_{max} approximated 17° at the slowest swimming speed, and smaller values were observed at faster swimming speeds (Fig. 12A). For the tail of *Micropterus salmoides*, α also fluctuated between positive and negative values within a single tail-beat cycle (Fig. 10). For trout and most other fish species with subcarangiform swimming and generalized tail morphology, few values of α are available. However, Bainbridge (1963) did measure α of goldfish (*Carassius auratus*) and dace (*Leuciscus leuciscus*) for both the distal caudal fin which ranged −6 to 12° and from −30 to 20°, respectively, and the caudal peduncle values ranged from −27 to 24° and from −21 to 18°, respectively. Using images spaced at approximately one-eighth of a tail-beat cycle, Bainbridge (1963) found $\alpha>0$ for about 75% of the tail-beat cycle for all regions of the tail, and that negative values of α were out of phase longitudinally such that the entire length of the tail always had at least one region with a positive angle of attack. In contrast, the proportion of the cycle with $\alpha>0$ in *Micropterus salmoides* varied longitudinally within the tail and was as small

as approximately 30 % of a cycle (Fig. 12C). Furthermore, slightly before the time of maximum lateral displacement of the tail tip in *Micropterus salmoides*, we found a time when α was simultaneously negative for both the proximal and distal portions of the tail (Fig. 11).

Angles of attack have been measured for other vertebrates with specialized tail morphologies and mechanisms of caudal propulsion. For example, during thunniform swimming of the tuna *Euthynnus affinis*, α of the tail was always positive and averaged about 30 ° as the tail crossed the axis of progression (Fierstine and Walters, 1968). Similarly, for bottlenose dolphins *Tursiops truncatus*, α of the flukes remains positive as it fluctuates within each tail-beat cycle, and mean α_{max} is greatest (approximately 20 °) at slowest speeds and declines linearly with increased swimming speeds (Fish, 1993). In the light of these results and the fact that the hypurals had $\alpha>0$ for a large portion of each cycle of *Micropterus salmoides*, it is possible that increased stiffness of caudal structures may facilitate the maintenance of positive angles of attack throughout the tail-beat cycle.

Additional factors affecting trailing edge orientation and angle of attack are the orientation and mechanical properties of nearby axial structures. For example, even for a rigid trailing edge, if the next most anterior structures have large values of θ, then the rigid trailing edge could have large values of θ (depending on the phase relationships between θ and the lateral flexion at the joint between the rigid and compliant structures). An underlying reason for large values of θ could also be low values of axial stiffness. For instance, as the caudal fin of *Micropterus salmoides* was pushed against the water, it had considerable lateral flexion (Fig. 6B) and, immediately posterior to the hypurals, there were large increases in the values of θ_{max} (Fig. 6C) relative to those of the hypurals. Considering the phase of lateral bending relative to lateral displacement, it seems likely that most of the observed bending of the caudal fin is a passive result of fluid resistance rather than a result of the activity of the musculature associated with the fin rays.

In addition to lateral vertebral flexion affecting muscle strain, as discussed previously, lateral vertebral flexion (strain) and its rate of change may also affect the stiffness within the vertebral column of a fish. The only dynamic measurements of intervertebral stiffness of fish are those of Long (1992), who studied the *in vitro* patterns of loading for pairs of vertebrae from the morphologically specialized backbones of marlin. Although *in vivo* estimates of lateral vertebral flexion were not available for this species, Long (1992) sinusoidally flexed vertebrae from several longitudinal locations at both 3 and 5 ° and at frequencies ranging from 0.5 to 5 Hz. Stiffness of the marlin vertebrae generally decreased with increased bending frequency, whereas it increased nearly twofold posteriorly and by about 30 % from 3 to 5 ° of bending. In the light of such intraspecific variation in stiffness, which was dependent on both longitudinal position and lateral bending, it should be especially interesting for future studies to determine these mechanical properties for additional species after *in vivo* estimates of vertebral flexion have been obtained.

The extent to which increased numbers of vertebrae may decrease overall axial stiffness remains unclear. Although direct estimates of lateral vertebral bending are not available for trout, the increased values of lateral displacement and θ_{max} (Webb *et al*. 1984; Webb, 1988) are changes in waveform that are consistent with greater curvature in the trout compared with *Micropterus salmoides*. Perhaps, greater curvature in the trout may indicate greater axial flexibility. Kinematic studies alone, with minimal information on internal anatomy, have proved extremely useful for estimating the power required for undulatory swimming and for predicting the design trade-offs in locomotor performance associated with different external shapes. However, additional comparative studies that carefully integrate internal axial morphology with kinematics and electromyography hold great promise for further clarifying the functional basis for kinematic similarity (or the lack of it).

We are grateful to J. Seigel and the Section of Fishes at the Los Angeles County Museum for the X-ray photography of specimens. H. Nguyen, J. Davis, A. Lozada and B. Malas laboriously digitized many video images. Support was provided by NSF grants BNS 8919497 to B.C.J. and G.V.L. and NSF BSR 9007994 to G.V.L. The high-speed video system was obtained under NSF BBS 8820664.

References

BAINBRIDGE, R. (1963). Caudal fin and body movement in the propulsion of some fish. *J. exp. Biol.* **40**, 23–56.

FIERSTINE, H. L. AND WALTERS, V. (1968). Studies of locomotion and anatomy of scombroid fishes. *Mem. south. Calif. Acad. Sci.* **6**, 1–31.

FISH, F. E. (1993). Power output and propulsive efficiency of swimming bottlenose dolphins (*Tursiops truncatus*). *J. exp. Biol*. **185**, 179–193.

FROLICH, L. M. AND BIEWENER, A. A. (1992). Kinematic and electromyographic analysis of the functional role of the body axis during terrestrial and aquatic locomotion in the salamander *Ambystoma tigrinum*. *J. exp. Biol.* **162**, 107–130.

GIBB, A., JAYNE, B. C. AND LAUDER, G. V. (1994). Kinematics of pectoral fin locomotion in the bluegill sunfish *Lepomis macrochirus*. *J. exp. Biol.* **189**, 133–161.

GRAY, J. (1968). *Animal Locomotion*. London: Weidenfield and Nicolson.

GRILLNER, S. AND KASHIN, S. (1976). On the generation and performance of swimming in fish. In *Neural Control of Locomotion* (ed. R. M. Herman, S. Grillner, P. S. G. Stein and D. G. Stuart), pp. 181–201. New York: Plenum Press.

JAYNE, B. C. (1988). Muscular mechanisms of snake locomotion: an electromyographic study of lateral undulation of the Florida banded water snake (*Nerodia fasciata*) and the yellow rat snake (*Elaphe obsoleta*). *J. Morph.* **197**, 159–181.

JAYNE, B. C. AND LAUDER, G. V. (1993). Red and white muscle activity and kinematics of the escape response of the bluegill sunfish during swimming. *J. comp. Physiol.* A **173**, 495–508.

JAYNE, B. C. AND LAUDER, G. V. (1994). Comparative morphology of the myomeres and axial skeleton in four genera of centrarchid fishes. *J. Morph.* **220**, 185–205.

LIGHTHILL, M. J. (1971). Large-amplitude elongated-body theory of fish locomotion. *Proc. R. Soc. Lond. B* **179**, 125–138.

LINDSEY, C. C. (1978). Form, function and locomotory habits in fish. In *Fish Physiology* (ed. W. S. Hoar and D. J. Randall), pp. 1–100. New York: Academic Press

LONG, J. H. (1992). Stiffness and damping forces in the intervertebral joints of blue marlin (*Makaira nigricans*). *J. exp. Biol.* **162**, 131–155.

MABEE, P. M. (1993). Phylogenetic interpretation of ontogenetic change: sorting out the actual and artefactual in an empirical case study of centrarchid fishes. *Zool. J. Linn. Soc.* **107**, 175–291.

ROME, L. C., FUNKE, R. P. AND ALEXANDER, R. MCN. (1990). The influence of temperature on muscle velocity and sustained performance in swimming carp. *J. exp. Biol.* **154**, 163–178.

ROME, L. C., FUNKE, R. P., ALEXANDER, R. MCN., LUTZ, G., ALDRIDGE, H., SCOTT, F. AND FREADMAN, M. (1988). Why animals have different muscle fibre types. *Nature* **335**, 824–827.

ROME, L. C. AND SOSNICKI, A. A. (1991). Myofilament overlap in swimming carp. II. Sarcomere length changes during swimming. *Am. J. Physiol.* **260**, C289–C296.

ROME, L. C., SWANK, D. AND CORDA, D. (1993). How fish power swimming. *Science* **261**, 340–343.

SCOTT, W. B. AND CROSSMAN, E. J. (1973). *Freshwater Fishes of Canada*. Ottawa: Fisheries Research Board of Canada.

STRANEY, D. O. (1990). Median axis methods in morphometrics. In *Proceedings of the Michigan Morphometrics Worshop* (ed. F. J. Rohlf and F. L. Bookstein), pp. 179–200. Ann Arbor: The University of Michigan Museum of Zoology. Special Publication No. 2.

VAN LEEUWEN, J. L., LANKEET, M. J. M., AKSTER, H. A. AND OSSE, J. W. M. (1990). Function of red axial muscles of carp (*Cyprinus carpio*): recruitment and normalized power output during swimming in different modes. *J. Zool., Lond.* **220**, 123–145.

VIDELER, J. J. AND HESS, F. (1984). Fast continuous swimming of two pelagic predators, saithe (*Pollachus virens*) and mackerel (*Scomber scombrus*): a kinematic analysis. *J. exp. Biol.* **109**, 209–228.

VIDELER, J. J. AND WARDLE, C. S. (1978). New kinematic data from high speed cine film recordings of swimming cod (*Gadus morhua*). *Neth. J. Zool.* **28**, 465–484.

WAINWRIGHT, S. A. (1983). To bend a fish. In *Fish Biomechanics* (ed. P. W. Webb and D. Weihs), pp. 68–91. New York: Praeger Publishers.

WEBB, P. W. (1975). Hydrodynamics and energetics of fish propulsion. *Bull. Fish. Res. Bd Can.* **190**, 1–159.

WEBB, P. W. (1982). Locomotor patterns in the evolution of actinopterygian fishes. *Am. Zool.* **22**, 329–342.

WEBB, P. W. (1988). 'Steady' swimming kinematics of tiger musky, an esociform accelerator and rainbow trout, a generalist cruiser. *J. exp. Biol.* **138**, 51–69.

WEBB, P. W. (1992). Is the high cost of body/caudal fin undulatory locomotion due to increased frictional drag or inertial recoil? *J. exp. Biol.* **162**, 157–166.

WEBB, P. W. (1993). The effect of solid and porous channel walls on steady swimming of steelhead trout *Oncorhynchus mykiss*. *J. exp. Biol.* **178**, 97–108.

WEBB, P. W., KOSTECKI, P. T. AND STEVENS, E. D. (1984). The effect of size and swimming speed on locomotor kinematics of rainbow trout. *J. exp. Biol.* **109**, 77–95.

WILLIAMS, T. L., GRILLNER, S., SMOLJANINOV, V. V., WALLÉN, P., KASHIN, S. AND ROSSIGNOL, S. (1989). Locomotion in lamprey and trout: the relative timing of activation and movement. *J. exp. Biol.* **143**, 559–566.

ZAR, J. H. (1984). *Biostatistical Analysis*. Englewood Cliffs, NJ: Prentice Hall.